HIGH VELOCITY PENETRATION OF STEEL TARGETS

B. R. Sorensen, K. D. Kimsey, G. F. Silsby, D. R. Scheffler, T. M. Sherrick
and W. S. de Rosset

Ballistic Research Laboratory, APG, MD 21005-5066, U.S.A.

Summary—Researchers at the U.S. Army Ballistic Research Laboratory (BRL) have conducted a combined experimental and numerical research program in high-velocity penetration aimed at increasing the understanding of penetration mechanics over the striking velocity range between 1.5 and 4 km/s. A judicious combination of ballistic tests and large-scale simulations have been used to evaluate the performance of a family of both monolithic and segmented penetrators against semi-infinite rolled homogeneous armor (RHA). The results of the experimental and numerical programs are discussed.

INTRODUCTION

The penetration mechanics and potential benefits of high-velocity for both monolithic and segmented penetrators have been examined in a combined experimental and numerical research program. The program consists of three parts: half-scale ballistic tests, full-scale ballistic tests and complementary computer simulations.

The half-scale firings were conducted at the von Karman G range of the U.S. Air Force Arnold Engineering Development Center (AEDC) by Calspan Corporation operating personnel. A large two-stage light gas gun was used to launch half-scale tungsten alloy penetrators at striking velocities from 2–4 km/s against semi-infinite RHA targets. The masses of the half-scale penetrators are nominally 1/8th that of the full-scale penetrators since the geometric scale factor is 1/2. The sabots for launching both the monolithic and segmented penetrators were designed by Calspan personnel.

The full-scale tests were conducted at the BRL using a double travel 120 mm M256 gun (9.5 m total travel) with a standard chamber. Preliminary design efforts showed that tungsten alloy (WA) cores with nominal masses of 1 and 2 kg with length-to-diameter ratios (L/D) of 20 could be launched with a double ramp aluminum sabot and achieve muzzle velocities of 2.5 and 2.3 km/s, respectively, with an optimized propelling charge. Two full-scale projectile geometries were selected: $L = 300$ mm, $D = 15$ mm, and $L = 380$ mm, $D = 19$ mm. Due to launch velocity limitations, the full-scale tests investigate the lower end of the velocity range. The full-scale tests provide baseline data against which the assumption of geometric scaling can be validated. The half-scale test series complements the full-scale series, generating penetration data at much higher velocities than possible at full-scale at this time.

Large-scale, finite-difference simulations were conducted and compared with experiments to establish the validity of the simulation approach, as well as to characterize high-velocity monolithic and segmented penetrator impact phenomenon against semi-infinite RHA. In many cases, direct comparisons with half-scale and full-scale test data are provided.

Figure 1 presents the target configuration for the semi-infinite RHA penetration tests. The full-scale target consisted of four 150 mm thick RHA plates welded together using eight mild steel straps (25 by 100 mm). In half-scale, eight retempered 75 mm RHA plates were welded together utilizing ASTM A36 2 by 2 by .375" structural angle (50 by 50 by 9.53 mm) on the corners. In both scales, the plates were nominally Brinell hardness (HBN) 269.

All tungsten penetrators were of nominal 90W-7Ni-3Fe alloy, Teledyne Firth Sterling X27, with the half-scale penetrators being produced by the small bar process. All bars were swaged to 18% reduction in area and strain aged 1 h at 400°C. The manufacturer
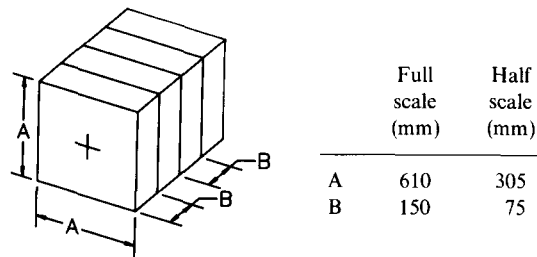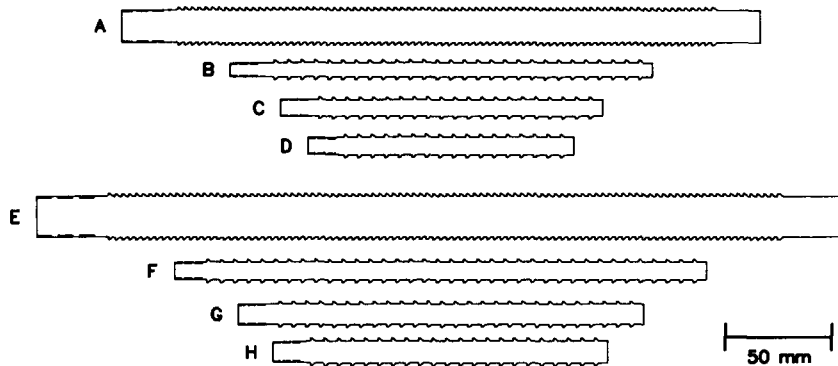
	Full scale (mm)	Half scale (mm)
A	610	305
B	150	75

FIG. 1. Semi-infinite RHA target configuration.

Penetrator type	Mass (g)	Minor diameter (mm)	Length (mm)	$\dfrac{L}{D}$	Scale
A	1020	15.00	300.0	20	Full
B	135	6.60	198.4	30	Half
C	140	7.57	151.4	20	Half
D	124	8.33	125.0	15	Half
E	2035	19.00	380.0	20	Full
F	262	8.33	250.0	30	Half
G	256	9.53	190.5	20	Half
H	247	10.49	157.4	15	Half

FIG. 2. Monolithic penetrator geometries.

reported mechanical properties for the half-scale penetrators of 1186 MPa tensile yield at the 0.2% offset, 1206 MPa tensile ultimate, 10.0% elongation to rupture, a Rockwell "C" hardness (HRC) of 41.5, and a density of 17.3 g/cc. The values for the full-scale penetrators were 1242 MPa, 1254 MPa, 7.0%, 42.0–42.4, and 17.3 g/cc, respectively. These mechanical properties are not significantly different from a similar material used in Silsby's AEDC firings in 1983 [1].

Six monolithic penetrator geometries were used for the half-scale tests: L/D of 15, 20 and 30 with nominal masses of 125 and 250 g. The geometric scale factor is one-half, e.g. the diameter of the $L/D = 20$, 125 g penetrator is half the minor diameter and length of the corresponding 1 kg full-scale penetrator. The penetrators consist of a basic cylinder with supercaliber driving lands and a 7075-T6 aluminum drag flare for stability. Due to manufacturing and launch considerations, the driving land profile for the full-scale penetrator is the minimum for ensuring launch integrity. The full-scale driving land profile was used for the half-scale penetrators with only slight modification and produces similar stress concentration factors, which is desirable. To avoid a disproportionately large ratio of outstanding driving land mass to cylinder mass compared to full-scale, every other driving land was removed on the half-scale penetrators; even so, resulting projectile masses vary from the nominal values. Figure 2 presents the monolithic penetrator geometries used for both the half-scale and full-scale tests.

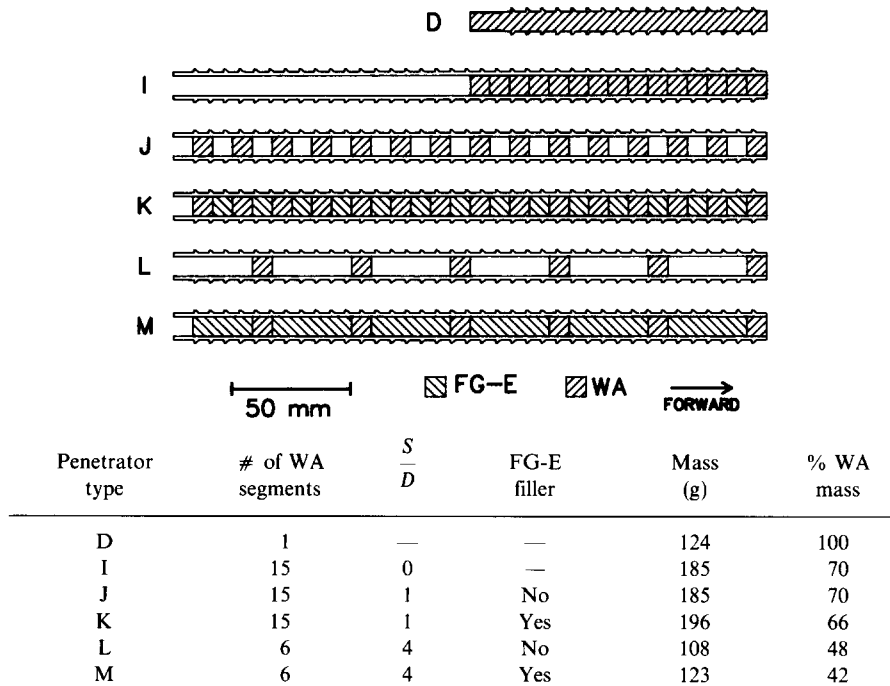| Penetrator type	# of WA segments	$\dfrac{S}{D}$	FG-E filler	Mass (g)	% WA mass
D	1	—	—	124	100
I	15	0	—	185	70
J	15	1	No	185	70
K	15	1	Yes	196	66
L	6	4	No	108	48
M	6	4	Yes	123	42

FIG. 3. Segmented penetrator geometries.

The work of others figured heavily in the design of the half-scale segmented penetrators. After examining the literature [2–7], a decision was made to parallel Cuadros' latest efforts at AEDC. The geometric configuration of cylindrical segments in a low density tubular carrier appears to alleviate many experimental and analytical problems reported in the literature; specifically, segment alignment, spindle contributions to penetration, and backstreaming debris [8,9]. Further benefits can be seen with the inclusion of a low density, relatively incompressible filler material (fiberglass–epoxy composite) between the segments. This addition reduces the upstream jetting of targer material inside the carrier tube as predicted by Hough [10].

Three segmented penetrator variants were examined in BRL's half-scale firings at AEDC: a baseline case comprised of 15 segments positioned in contact, flush with the forward end of the overall projectile; a case with 15 segments equally spaced one segment length apart; and a case with six segments spaced four segment lengths apart. Two alternate conditions were examined in the latter cases. The space between the individual segments was either left empty or filled with a fiberglass–epoxy filler plug. The individual segments are externally threaded to 3/8-24 UNF (nominally 8.33 mm in diameter) and were machined to a length of 8.33 mm. These were screwed into a 250 mm long, 12.7 mm basic minor O.D. 7075-T6 aluminum carrier tube with the same driving land profile used for the monolithic penetrators. An aluminum drag flare is screwed into the rear and projects and additional 5.33 mm behind the rear of the carrier tube. Figure 3 presents a schematic of the segmented penetrator geometries used for the half-scale tests.

In this and all following discussions of semi-infinite penetration results, only data from "good" shots are presented. The actual criteria by which the results of a shot are accepted or rejected are based on striking location and orientation. First, the impact must be located on the target in such a manner that no free edges are disturbed. Secondly, the critical combined pitch and yaw above which data are disregarded occurs when the side of the rod interferes significantly with the penetration channel and/or the entrance hole. The acceptance criteria is presented in detail in a BRL report in preparation [11]. Critical yaw can be reduced to a function of L/D and striking velocity. Buried within these terms are other terms like hole size, which is a function of penetrator diameter, materials and striking velocity. For the penetrator–target combination of 90–93% WA vs RHA steel, Fig. 4
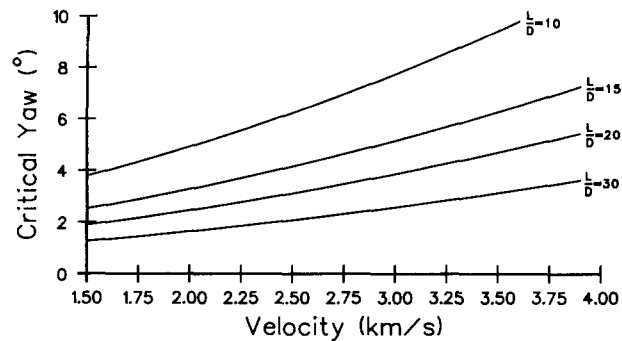
FIG. 4. Critical yaw as a function of impact velocity and penetrator L/D for 90–93% WA impacting 0° RHA steel [11].

TABLE 1. PERFORMANCE OF X27 WA PENETRATORS VS SEMI-INFINITE RHA

Shot #	$\frac{L}{D}$	Nominal mass (g)	Striking velocity (km/s)	Striking pitch (°)	Striking yaw (°)	Penetration (mm)
6260*	15	125	4.01	2.0	3.1	194
6261*	30	250	2.96	0.8	3.1	382
6289	15	125	2.89	0.5	−0.2	186
6290	20	125	2.90	2.2	2.6	220
6291	30	125	3.02	−0.2	−0.8	287
6296	15	125	2.98	0.2	−1.0	188
6297	15	125	2.99	1.2	0.7	189
6298	20	125	2.98	−1.0	1.2	229
6299	20	125	3.02	1.8	1.3	230
6313	20	125	2.42	0.0	0.0	220
6314	20	250	2.18	−0.5	−2.6	250
6315	30	125	3.05	−2.0	−2.0	292
6316	20	125	2.41	3.0	−1.0	214
6317	20	125	2.33	0.0	−0.6	210
6328	20	250	2.14	1.8	1.0	244

*Bar target.

represents critical yaw as a function of velocity and L/D. For a given L/D penetrator striking at a specified velocity, any combined yaw less that the critical yaw will provide data with minimal yaw affects. The ultimate test of data validity in yawed impact remains in the visual inspection of the penetration channel. In all cases of questionable yaw, the penetration was inspected to confirm data quality.

EXPERIMENTAL RESULTS

Half-scale results

Semi-infinite RHA penetration by monolithic penetrators. The results of the half-scale firings of monolithic rods against semi-infinite RHA provide a baseline against which the performance of the segmented penetrators are judged. The data are presented in Table 1. Two shots were fired initially for checkout and calibration into bar targets used in earlier work [1]. Bars 150 mm square by 600 mm long were cut from plate; thus, penetration was in the rolling plane rather than normal to it. The rest of the targets were laminated stacks of RHA as previously described.

To provide a feeling for the quality of the data, Fig. 5 shows the tabulated penetration data (after normalizing by the initial penetrator length, i.e. P/L) plotted with published and unpublished data for 90% WA long rods vs semi-infinite steel armor [1,2,4,12–15]. This data set consists of L/D's ranging from 9 to 30 with densities from 17.0 to 17.6 g/cc.
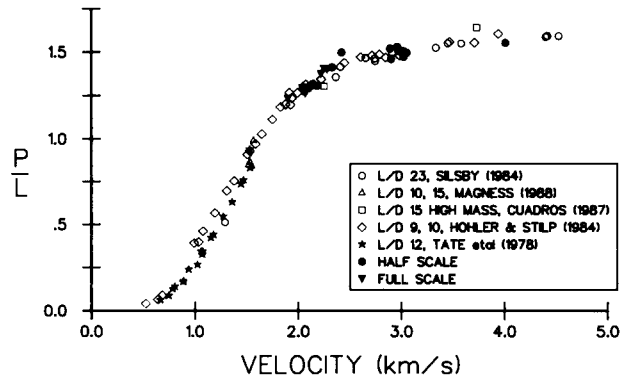
FIG. 5. Semi-infinite RHA penetration by 90% WA monolithic penetrators.

TABLE 2. PERFORMANCE OF X27 WA SEGMENTED PENETRATORS VS SEMI-INFINITE RHA

Shot #	Number segments	Penetrator description	$\dfrac{S}{D}$	FG-E filler	Striking velocity (km/s)	Striking yaw (°)	Striking pitch (°)	Penetration (mm)
6343-1	1	Sphere	—	—	2.84	—	—	16.0
6343-2	1	Sphere	—	—	2.84	—	—	16.5
6343-3	1	Sphere	—	—	2.84	—	—	17.5
6433	6	Eq. space	4	Yes	3.00	−1.0	0.7	158
6434	6	Eq. space	4	Yes	3.05	0.5	0.8	157
6333	15	All forw	0	—	2.95	−0.4	−0.1	211
6335	15	All forw	0	—	3.00	−2.5	0.8	213
6332	15	Eq. space	1	No	2.94	−3.0	0.5	238
6334	15	Eq. space	1	No	3.02	0.5	−0.3	238
6337	15	Eq. space	1	Yes	3.01	−1.6	1.0	272
6339	15	Eq. space	1	Yes	3.03	−3.0	1.0	264

*FG-E indicates fiberglass–epoxy filler.

Typical rod masses are 100 g or less, although there are three shots from Cuadros for rods approaching a kilogram. It is easily observable that the half- and full-scale data are comparable with data from the literature; further analysis of these data will follow.

Semi-infinite RHA penetration by segmented penetrators. The data for the half-scale segmented penetrator tests are given in Table 2. It should be noted that the data for the six equally spaced segments without filler were disregarded due to excessive yaw. Furthermore, a single shot of five tungsten spheres 8.33 mm in diameter was fired to provide a semi-infinite penetration baseline for an individual segment. However, only three of the spheres had impact locations providing useable data. The penetration of these spheres was considerably less than the data for L/D one cylinders reported in Ref. [14]. This can most likely be attributed to the sphere's lower mass compared to that of a cylinder of the same diameter. A short series of tests with 25.4 mm diameter sphere and cylinder shots are underway to resolve this issue.

Full-scale tests

The projectiles were designed to integrate into a 120 mm cartridge system. Design work was completed on an automated CAD network utilizing 3D drafting and finite element analysis. A 2D, axisymmetric, quasistatic model was used for the inbore analysis. A 3D static analysis of sabot integrity at discard was also performed. No windshield was used and a six blade uncanted fin was added for flight stabilization. The design effort was conservative to insure a good launch and discard. Final production weights of the two projectiles were 3.5 and 4.9 kg. Interior ballistic calculations estimated that the muzzle

TABLE 3. PERFORMANCE OF X27 WA, L/D 20 PENETRATORS VS SEMI-INFINITE RHA

Shot #	Mass (kg)	Velocity (km/s)	Yaw (°)	Pitch (°)	Penetration (mm)
2395	2.0	2.05	1.8	1.4	484
2396	2.0	2.07	0.1	2.3	480
2398	1.0	2.22	0.6	−0.8	412
2399	1.0	2.12	1.2	−1.7	389
2401	1.0	2.25	0.2	1.0	421
2402	1.0	2.28	−1.2	0.3	420
2403	2.0	2.06	0.3	<0.7	486
2410	2.0	1.90	0.7	0.3	468
2413	1.0	2.04	0.1	−0.7	388

velocities would be approximately 2.4 and 2.2 km/s, respectively. The drop-off from the desired velocities of 2.5 and 2.3 km/s was due to the use of a non-optimized charge.

The testing was done at the BRL's Transonic Range. The gun tube was mounted on a M110A carriage with a M256 breech. The instrumentation consisted of one orthogonal set of muzzle X-rays, four smear cameras (6.5 to 70 m), a down bore camera, yaw cards (5 m intervals) after the stripper plate and orthogonal striking X-rays (one horizontal, two vertical). To evaluate the charges, several slugs of each weight were tested initially. Two to three shots of each projectile were fired to determine yaw characteristics. Once adequate yaw data were obtained, the gun was moved to the proper distance to minimize yaw at the target, and the remaining test entries completed.

The maximum velocities attained for each projectile were 2.28 and 2.07 km/s. This was only accomplished after heating the propellant to increase the breech pressure to over 690 MPa. The interior ballistic calculations indicated that velocities of 2.4 and 2.2 km/s should have been obtained with the ambient charge. This discrepancy is most likely due to an apparent increase in projectile/tube resistance as compared to that at normal ordnance velocities (1.4–1.7 km/s). This important issue is being addressed by others [16].

Examination of the photographic and radiographic data show excellent launch characteristics: clean sabot separation with the petals maintaining their integrity until clear of the subprojectile. Straight penetrators were observed at muzzle and target. The 1 kg penetrator displayed severe fin damage; bent and/or missing blades at the muzzle and excessive ablation at the target. The bending was probably caused by thermal softening while pulling through the propellant bed. This damage caused inconsistent yaw and dispersion. The fins were coated with 1–3 mm of jRTV rubber to provide thermal protection. After this was done, all evidence of fin damage disappeared. There was also some inconsistency in the yaw period for the 2 kg penetrator, but no explanation could be found. Once initial problems were overcome, accuracy, dispersion and yaw were acceptable for both projectiles.

Tabulated in Table 3 are the data for the firings against semi-infinite RHA. Yaw, pitch and velocity are measured from radiographs taken two meters uprange of the target. The data are plotted in Fig. 5 along with the half-scale results. This plot of normalized penetration against velocity shows that normalized full-scale performance is similar to that of the half-scale.

ANALYSIS OF EXPERIMENTAL RESULTS

Monolithic penetration in semi-infinite RHA

Penetration of monolithic rods into semi-infinite RHA depends strongly on striking velocity and rod length. To be able to observe second order effects, such as the influence of P/L and mass, the first order effects must be quantified and removed from the observed performance. To do this, the extant data cited earlier (Fig. 5) for 90% WA long rods vs semi-finite armor steel at striking velocities from 1–5 km/s were normalized by the initial
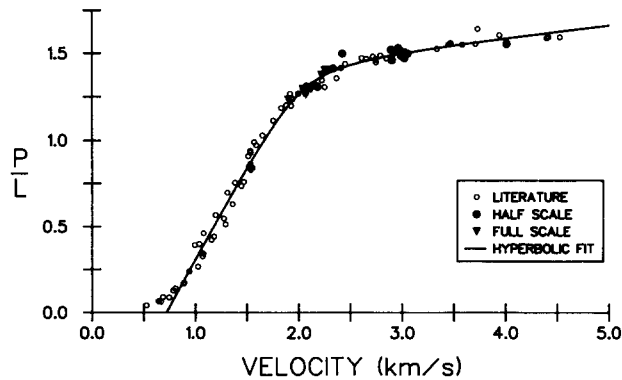
FIG. 6. Hyperbolic fit and semi-infinite penetration data.

rod length (P/L) and the resultant data set was fit with a curve as a function of striking velocity (see Fig. 6).

Over this spread of striking velocities, the data are recognized as having a sigmoid shape. A small initial upward-curving portion rises with increasing velocity from zero penetration, giving way to a steep, essentially linear rise over the ordnance velocity regime (1–2 km/s). A downward curved region connects to a second linear region with a low slope, crossing the hydrodynamic limit (i.e. the density law) at about 3 km/s. Ignoring the very low velocity regime (<0.75 km/s), the behavior is suggestive of a hyperbola.

The statistical adviser expert system RS/1 [17] was used to fit the extant data to a generalized conic-section. From the fitted curve, the data residuals were calculated. The residuals were examined and found to be symmetric, normally distributed, and without any systematic trend with velocity, suggesting that the form of the curve is acceptable. It should be understood that the fitted curve is not intended to be used as a generalized penetration model, but as an analytical tool to compare the three data sets. Figure 6 plots the hyperbolic fit against the extant and experimental data.

The half- and full-scale data were then compared to the extant data and to each other to determine if any statistically significant trends could be determined. Student's t-test at a confidence level of 0.05 was utilized to compare differences within the data sets. There was no statistically significant difference between either the half- or full-scale data and the extant data. Furthermore, there was also no significant difference between the half- and full-scale data. Thus, for a range of rod masses of over an order of magnitude, the effect of scale on semi-infinite penetration is insignificant. It should be noted that "no significant difference" does not mean that there is no difference, but rather that whatever difference may exist is too small compared to the scatter in the data to be detected given the number of experimental data points. Furthermore, a confidence level of 0.05 roughly means that one time in 20 the conclusion is wrong.

It is known that P/L depends on L/D for L/D's from 1 to 10, but with the effect becoming less important as L/D increases beyond 10. Statistical tests were performed on the experimental data to investigate if there is a dependence on L/D for L/D's 15 to 30. The experimental data from the half-scale 125 g penetrators were divided into their respective L/D categories. The data from each category were statistically analysed with no significant differences being found. In particular, the difference between the L/D 15 and the L/D 30 data, where such a difference would be most observable, was insignificant.

Segmented penetrators against RHA

Analysis of the results of the segmented penetrator firings versus semi-infinite RHA are presented in Fig. 7. Figure 7 also includes data from [2–4] segmented penetrator firings conducted at AEDC. This figure represents normalized penetration (P/L_{WA}) against normalized segment separation (S/D). The scheme for computing normalized penetration is different that that as described earlier for monolithic penetrators. In this case, the total collapsed length of the WA elements is used as L_{WA}. This is one of many different methods
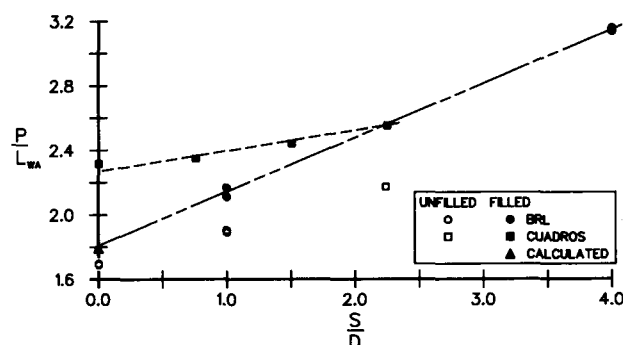
FIG. 7. Normalized penetration vs normalized separation for X27 WA segments in Al carrier tubes.
Impact velocity: 3.0 km/s.

in which the performance of segmented penetrators can be presented and does a sufficient job of delineating trends in this case. One important configuration was not tested: 15 WA segments, forward with no separation, with filler material behind the segments (penetrator type I in Fig. 3 but with filler). To assist in analysis, this configuration was simulated numerically to provide data for establishing trends.

With this combined data set, several trends can be noted. Performance increases as the separation increases. The presence of filler improves the performance dramatically, lending credence to either the hypothesis that armor and/or penetrator material jetting reduces segment performance, or the filler material alone contributes significantly to penetration. Lastly, the effect of segment L/D appears to influence the slope of the response. Cuadros' design with L/D 1.5 segments shows considerably less improvement with separation than does the BRL design with L/D 1 segments.

LARGE-SCALE CONTINUUM SIMULATIONS

The HULL code [18,19] has been used to model many of the half-scale and full-scale tests. HULL is a family of computer programs for solving continuum dynamics problems. The code solves the finite difference analogs of the governing partial differential equations for two- and three-dimensional Eulerian and Lagrangian formulated problems as well as coupled Eulerian/Lagrangian solutions. Most solids in HULL are modeled with the Mie–Gruneisen equation of state. Material failure models include: maximum principal stress, maximum principal strain, and the Hancock–Mackenzie triaxial failure model [20]. When material failure occurs a numerically significant volume fraction of air is introduced in the cell which permits relaxation of the tensile stresses to the yield surface. Recompression is permitted.

The simulations reported herein have used the Mie–Gruneisen equation of state to model the hydrodynamic behavior. The coefficients for the equation of state data were obtained from Ref. [21]. The deviatoric or shear behavior has been modeled with an incremental elastic–plastic formulation following the description given by Wilkins [22]. An elastic-perfectly plastic model has been used for the RHA with a 719 MPa yield strength [23]. A strain-hardening plasticity model was used for the tungsten alloy with an initial yield strength of 1418 MPa and an ultimate strength of 1955 MPa at 3.1% strain [24]. For the segmented penetrator simulations the 7075-T6 aluminum carrier tube was modeled with a constant yield strength of 770 MPa [24]. A constant yield strength of 628 MPa was used for the epoxy-fiberglass filler [25].

Table 4 presents the computed penetration for both the half- and full-scale monolithic penetrators impacting semi-infinite RHA. The computed penetrations presented in Table 4 are in good agreement with the half- and full-scale test data for those shots with an acceptable yaw; direct comparison with test data are not provided for shots with unacceptable yaws since axisymmetric computations were performed. In addition, the predicted penetrations are consistent with other data reported in the literature [2,4,12–15].

TABLE 4. COMPUTED AND MEASURED PERFORMANCE OF X27 WA MONOLITHIC PENETRATORS IMPACTING SEMI-INFINITE RHA

| Shot #	$\dfrac{L}{D}$	Mass (g)	Striking velocity (km/s)	Measured penetration (mm)	Computed penetration (mm)	Difference (%)	Computed $\dfrac{P}{L}$
6313	20	125	2.5	225	221	1.8	1.42
6299	20	125	3.0	228	235	3.1	1.52
	20	125	3.5		243		1.57
	20	125	4.0		249		1.61
6314	20	250	2.2	249	258	3.6	1.32
	20	250	2.5		278		1.43
	20	250	3.0		296		1.52
	20	250	3.5		306		1.50
6220	15	125	3.0	194	201	3.6	1.57
6315	30	125	3.0	297	289	2.7	1.43
2402	20	1000	2.3	420	400	5.0	1.32
2403	20	2000	2.0	486	495	1.9	1.20
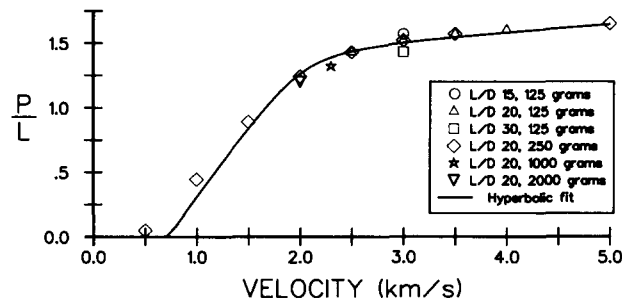
FIG. 8. Predicted and measured performance of X27 WA penetrators vs semi-infinite RHA.

Figure 8 presents the computational results overlaid on the hyperbolic fit to the extant data discussed earlier. The only disparity occurs at velocities below 1 km/s. This is understandable since the velocity threshold for the data used in creating the hyperbolic fit was approximately 1 km/s and above. Therefore, it would be unreasonable to expect the curve to represent events below the velocity threshold as demonstrated in Fig. 6.

Monolithic penetrators. Figure 9 shows the computational results contrasted with the experimental data from this work. The correspondence with the data is excellent. Statistical analysis of the residuals revealed no significant difference between the mean of the computational residuals and the half- and full-scale data sets. The star symbol (Fig. 9) is actually an overlapping solid-square and a solid-diamond, indicating that there is no difference between the computational results for the 125 and 250 g L/D 20 rods. Furthermore, the computational results show a variation in performance with L/D. The 125 g penetrators at 3.0 km/s show a decrease in P/L as L/D increases from 15 to 30. This variation has also been observed in ballistic tests and analytical studies of impact [14,26]. An explanation for this disagreement with the experimental results mentioned earlier is the computational method produces the same data for replicated test entries; whereas the experimental data will have scatter. Examinations of Fig. 9 verifies this statement. The noise in the experimental data is of the same magnitude as the signal, effectively masking any differences as already discussed. Regardless of the slight discrepancy in P/L vs L/D, the overall close correspondence of the computed penetrations with the experimental data clearly demonstrates the validity of large-scale simulations for modeling high-velocity impact of semi-fininite RHA targets.

Segmented penetrators. The performance of four segmented penetrator geometries was modeled for comparison with the half-scale firings at AEDC. The segmented penetrator
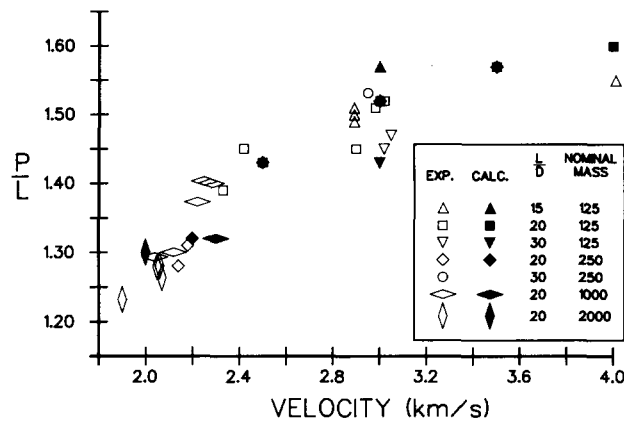
FIG. 9. Predicted and measured performance of X27 WA penetrators vs semi-infinite RHA. Note that the L/D 20, 125 g and L/D 20, 250 g penetrators yield identical P/L for the same striking velocity.

TABLE 5. 125 g SEGMENTED PENETRATORS VS SEMI-INFINITE RHA, STRIKING VELOCITY 3.0 km/s

Shot #	Penetrator description			Measured penetration (mm)	Calculated penetration (mm)	Difference (%)
	#	S/D	Filler			
6332	15	1	No	237	228	3.8
6347	6	4	No		138	
6337	15	1	Yes	272	265	2.5
6333	1	—	No	212	216	1.8

model included the 7075-T6 aluminum carrier tube ($L/D = 30$, minor O.D. 12.7 mm, I.D. 8.33 mm). The specific segmented penetrator geometries modeled include a baseline L/D 15 tungsten alloy penetrator positioned flush with the impact face of the carrier tube, 15 L/D 1 segments spaced at once projectile diameter (8.33 mm) without any filler, material between the individual segments, 15 L/D 1 segments spaced one projectile diameter apart with epoxy–fiberglass filler between the individual segments, and 6 L/D 1 segments spaced four projectile diameters apart without any filler material between the individual segments.

The penetration predicted by the axisymmetric simulations are presented in Table 5, and are compared with the data obtained from the firings at AEDC. There exists good agreement between the experimental and the computational data, which suggests that large-scale continuum models are a valid technique for predicting the performance of high-velocity segmented projectiles striking semi-infinite steel targets (provided dynamic material properties are available for the materials of interest). No direct comparison is available for the six segment ($S/D = 4$) projectile, due to high impact yaw.

Both the experimental and the computational data show that placing epoxy–fiberglass filler between the individual segments increases total penetration over the unfilled case by approximately 14%. While the epoxy–fiberglass material increases the mass of the penetrator slightly, which contributes to the total penetration, this is felt to be a secondary affect. The computations suggest that the performance of the non-filled segmented penetrator is primarily degraded by carrier tube material flowing into the region between the individual segments, see Fig. 10. Furthermore, the penetration mechanism of the carrier tube between individual segments is analogous to a tubular penetrator, i.e. a portion of the tube-wall material flows to the outside and the remaining tube-wall material and target material flows to the inside cavity. This phenomenon has been documented in analytical and hydrocode simulations in Refs [10,28]. In addition, the filler material also excludes erosion products from entering the space between individual segments, thereby decreasing the amount of material penetrated.
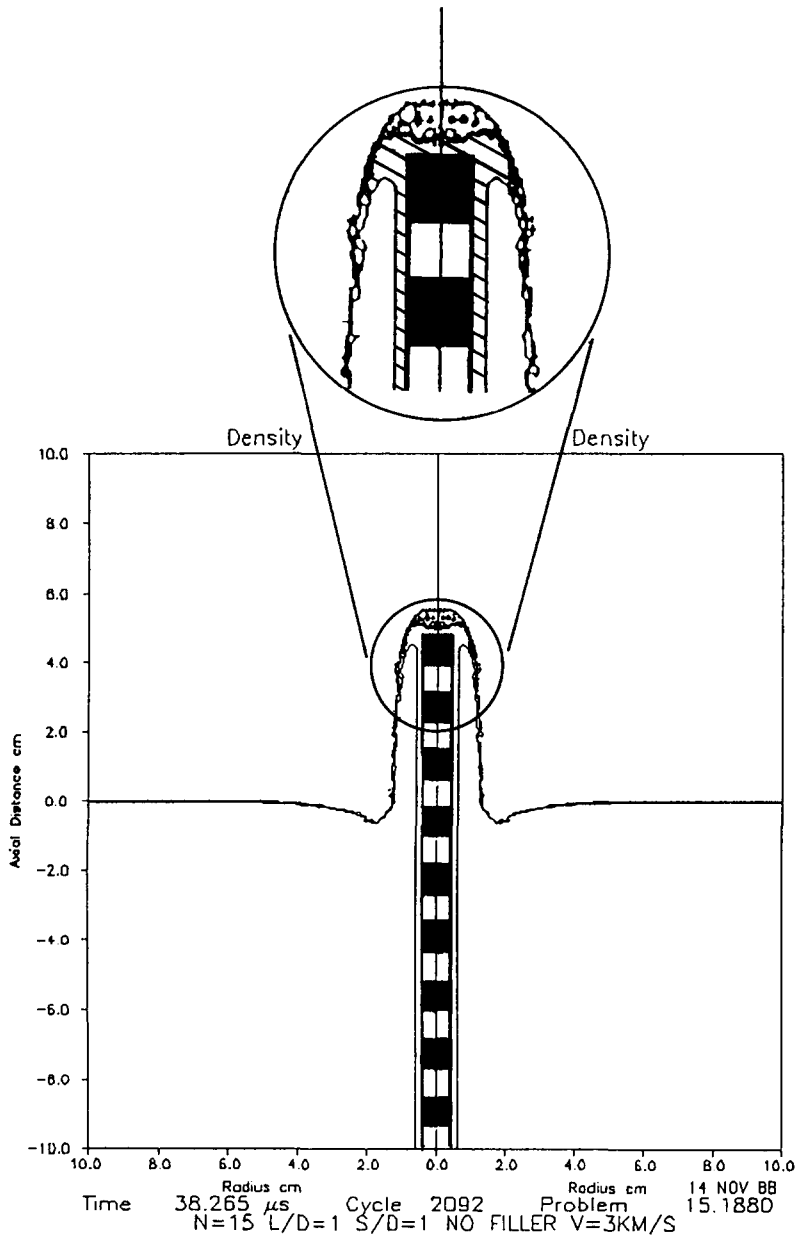
FIG. 10. Segmented rod penetration at 38 ms. Striking velocity is 3 km/s. WA segments are shaded. Aluminum carrier tube is cross-hatched. Note intrusion of aluminum carrier tube material between leading segments.

CONCLUSIONS

The penetration mechanics and potential benefits of high-velocity have been examined in a combined experimental and numerical research program. Through the judicious combination of ballistic tests and large-scale simulations, BRL researchers have evaluated the performance of both monolithic and segmented penetrators against semi-infinite RHA at striking velocities between 2 and 4 km/s. The data obtained from the half- and full-scale ballistic tests, as well as from the large-scale simulations suggest a number of conclusions.

The penetration results for monolithic WA rods impacting semi-infinite RHA agree with previously published data for high velocity impacts. The half- and full-scale data of monolithic WA rods impacting semi-infinite RHA demonstrate that penetration does scale across a factor of two. The simulation approach has been validated for high velocity impact

of semi-infinite RHA, provided dynamic material properties are used. Excellent agreement, typically within 5%, was observed for both monolithic and segmented penetrator impacts. While the simulations show a L/D trend (see Fig. 9), the scatter in the experimental data is such that the effect is masked. The penetration performance of the segmented rods against the semi-infinite RHA targets was not as great as might be expected if the total penetration were simply the sum of the expected contributions from individual segments. For the segmented rod geometries investigated, the segmented rod out-performed a similar length/mass/diameter monolithic rod by 13% at 3 km/s. Part of the explanation for the under-performance is suggested by the large-scale simulations which show that some of the segments were forced to penetrate aluminum carrier material in addition to target material. Recent calculations and ballistic tests [28–30] suggest that a larger segment spacing should increase the total penetration.

REFERENCES

1. G. F. SILSBY, Penetration of semi-infinite steel targets by tungsten long rods 1.3 to 4.5 km/s. *Proc. Eighth Int. Symp. Ballistics*, October (1984).
2. J. H. CUADROS, General Dynamics Corporation (GD), Pomona Division. Segmented projectile experiments at 3.7 km/s, December 1985 to January 1987. Briefing at US Army BRL, 3 September (1987).
3. J. H. CUADROS, GD Pomona Division. Telephone conversations with G. Silsby of the BRL and subsequent correspondence concerning results of GD's in-house research on hypervelocity impact, supporting their electromagnetic gun project for tank main armament, 27 May (1987).
4. L. P. BELL, Evaluation of segmented and solid rod projectiles during hypervelocity flight and impact. Arnold Engineering Development Center TSR-87-v6, Arnold AFB, TN, March (1987).
5. A. C. CHARTERS, The penetration of RHA by continuous and segmented rods at high velocity: theory and experiments. General Research Corporation (GRC) CR-87-1008, Santa Barbara, CA, December (1986).
6. A. C. CHARTERS, GRC. Telephone conversation with G. G. Silsby of BRL, July–August (1989).
7. A. C. CHARTERS and T. L. MENNA, GRC. DARPA A/AA Program briefing presented at the Impact Physics Team Second Quarterly Review, Lawrence Livermore National Laboratory, 14–15 October (1987).
8. D. R. SCHEFFLER, Two-dimensional computer simulations of segmented penetrators impacting semi-infinite steel targets. *Int. J. Impact Engng* 9, 35–43 (1990).
9. G. L. HAUVER, BRL. Personal communication with G. Silsby (1987).
10. G. L. HOUGH, Hydrocode Analysis of Tubular KE Penetrators. Air Force Armament Laboratory TR-82-85, Eglin AFB, FL (1982).
11. T. BJERKE, G. F. SILSBY, D. R. SCHEFFLER and R. M. MUDD, Yawed long-rod armor penetration at ordnance and high velocities. BRL Technical Report, to be published.
12. A. TATE, K. E. B. GREEN, P. G. CHAMBERLAIN and R. G. BAKER, Model scale experiments of long rod penetration. *Proc. Fourth Int. Symp. Ballistics*, October (1978).
13. D. R. CHRISTMAN and J. W. GEHRING, Semiannual Report on Penetration Mechanics of High Velocity Projectiles. General Motors Corporation Defense Research Laboratories, TRR63-250, Santa Barbara, CA, September (1963).
14. V. HOHLER and A. STILP, Influence of length-to-diameter ratio in the range from 1 to 32 on the penetration performance of rod projectiles. *Proc. Eighth Int. Symp. Ballistics*, October (1984).
15. L. S. MAGNESS, BRL. Private communications to G. F. Silsby. Data from penetration materials program (1988).
16. F. ROBBINS, BRL. Private communications on the full-scale velocity predictions and firing data, April (1989).
17. BBN Software Products Corporation, RS/1 Release 3.0 User's Manual (1987).
18. D. A. MATUSKA and J. J. OSBORN, HULL Technical Manual, Vol I, Orlando Technology Incorporated (1986).
19. D. A. MATUSKA and J. J. OSBORN, HULL Users Manual, Vol II, Orlando Technology Incorporated (1986).
20. J. W. HANCOCK and A. C. MACKENZIE, *J. Mech. Phys. Solids* 24, 147 (1976).
21. B. J. KOHN, Compilation of Hugoniot Equations of State. Air Force Weapons Laboratory TR-69-38, Wright Patterson AFB OH, April (1969).
22. M. L. WILKINS, in *Methods in Computational Physics* (edited by B. Adler *et al.*). Academic Press, New York (1964).
23. R. V. BENCK and J. ROBITAILLE, Tensile stress–strain curves—III, rolled homogeneous armor at a strain rate of 0.42 s^{-1}. Ballistic Research Laboratory Memorandum Report BRL-MR-2760, July (1977).
24. T. NICHOLAS, Dynamic tensile testing of structural materials using a split Hopkinson bar apparatus. Air Force Wright Aeronautical Laboratories TR-80-4053, Wright Patterson AFB, OH, October (1980).
25. G. SILSBY, BRL, Private communication, June (1988).
26. K. FRANK and J. ZOOK, Energy efficient penetration and performance of targets in the hypervelocity regime. *Int. J. Impact Engng* 5, 277–284 (1987).
27. R. R. FRANZEN, Notes on tubular hypervelocity penetrators. *Proc. Tenth Int. Symp. Ballistics*, Vol II, American Defense Preparedness Association, October (1987).

28. J. A. ZUKAS, Numerical simulation of semi-infinite target penetration by continuous and segmented rods. BRL-TR-3081, February (1990).
29. A. C. CHARTERS and T. L. MENNA, GRC. DARPA A/AA Program briefing presented at the Impact Physics Group Fourth Program Review, DOE, Albuquerque, NM, 23–24 May (1988).
30. D. L. ORPHAL and R. R. FRANZEN, Penetration mechanics and performance of segmented rods against metal targets. *Int. J. Impact Engng* **10**, 427–438 (1990).